Astronomy & Astrophysics manuscript no. ms
December 29, 2022

The eclipse of ASASSN-21qj

Matthew A. Kenworthy[1], Arttu Sainio[1], Eric E. Mamajek[1], Joeseph Masiero[1], Amy Mainzer[1], Joeseph (Davy) Kirkpatrick[1], Richelle F. van Capelleveen[1], Grant M. Kennedy[1], Ludmila Carone[1], NEOWISE authorship list[1], AAVSO observers[1], Stéphane Charbonnel[1], Olivier Garde[1], Pascal Le Dû[1], Lionel Mulato[1], and Thomas Petit[1]

Leiden Observatory, University of Leiden, PO Box 9513, 2300 RA Leiden, The Netherlands
e-mail: kenworthy@strw.leidenuniv.nl

Received XXXX; accepted XXXX

ABSTRACT

Context. Collisions occur between planetessimals that generate debris disks through collisional cascades.
Aims. We analyze the dust and size distribution of the eclipse seen towards ASASSN-21qj.
Methods. Fit the light curve from three different colours to determine the particle size and distribution.
Results. The eclipse is coloured, indicating dust. The dust has a lower limit mass of XXXX Earths, eclipse has a duration of XXXX days.

Key words. giant planet formation – κ-mechanism – stability of gas spheres

1. Introduction

Terrestrial planets are thought to be built up by the quasi-periodic accretion of planetary embryos that generate a significant amount of ejected material. The Earth's moon is believed to have formed from the resulting aftermath of a collision in the early Solar system. Sudden increases of infrared flux from systems known to host debris disks indicate that this is a stochastic process that can occur on timescales of a few months or less. Models of these impacts and the subsequent evolution of the dust clouds have been modeled (Jackson & Wyatt 2012; Jackson et al. 2014) and have been seen at IR wavelengths (Su et al. 2019, 2022).

The star 2MASS J08152329-3859234 underwent a sudden dimming event in December 2021, which was announced by Rizzo Smith et al. (2021) and assigned the identifier ASASSN-21qj, which we will subsequently use for the rest of this paper. The star has undergone rapidly fluctuating photometry through to August 2022 (Rizzo Smith et al. 2022) and has been monitored intensively by the AAVSO observers and the LCOGT network of telescopes. It had previously shown no significant stellar variation in the optical bands for 2300 days as reported in Rizzo Smith et al. (2021). Searches through other photometric archives showed no significant changes in the optical bands before this epoch. The wide field infrared satellite WISE has photometric imaging from 3.8 microns (band W1) through to 22 microns (band W4), and the NEOWISE survey has photometry for bands W1 and W2 for this star. This star showed a significant brightening of 0.4 magnitudes in W1 and 0.8 magnitudes in W2 between two observing epochs (58055 MJD and 58245 MJD), and the IR color of the star had changed from W1-W2=0.0 to 1.2, but no significant changes in flux in the optical bands were seen during this time. Some 900 days later, the dimming was seen in the optical, and the absorption is larger at shorter optical wavelengths. These observations are all consistent with an event that generated a significant amount of sub-micron dust which subsequently started to transit the stellar disk.

We hypothesise that there was a collision between one or more rocky bodies in the system which generated a significant amount of dust, which has then subsequently begun to transit the star. This is consistent with a late type impact between a planet and large asteroid, similar to the one that generated the Earth/Moon system.

The structure of our paper is as follows: the analysis of the star is given in Section 2, the observations are detailed in Section 3, and we make an estimate of the physical parameters of the hypothesised dust cloud in Section 4. We then place this model in the context of planet formation in Section 5 and summarise the paper in Section 6.

2. Properties of the star

The properties of ASASSN-21qj are listed in Table 1. Photometry from various sources was compiled and analysed using the Virtual Observatory SED Analyzer (VOSA; Bayo et al. 2008) and the results are listed in Table 1, showing that ASASSN-21qj is consistent with being a G2 type dwarf star.

2.1. Possible multiplicity of ASASSN-21qj

ASASSN-21qj (Gaia DR3 5539970601632026752 = 2MASS J08152329-3859234) has a neighbor (Gaia DR3 5539970597334497024 = 2MASS J08152298-3859244) which is a visual double (see Figure 3). Based on the Gaia EDR3 mean ICRS position for epoch 2016.0, the visual companion lies at a separation ρ = 3738.243 ± 0.062 mas and at position angle $\theta = 249°.977$. Their parallaxes (ϖ = 1.7631 ± 0.0112 mas vs. 1.4711 ± 0.0523 mas) differ by 5.5σ and proper motions (μ_α = −9.692 ± 0.012, μ_δ = 7.349 ± 0.012 mas yr^{-1} vs. μ_α = −0.114 ± 0.055, μ_δ = 6.419 ± 0.053 mas yr^{-1}) differ by a factor of 2. If the two stars are at the parallactic distance of ASASSN-21qj (d = 552.4 pc; Bailer-Jones et al. 2021), then their difference in proper motion ($\Delta\mu$ = 9.623 ± 0.056 mas yr^{-1})

Table 1. Properties of ASASSN-21qj

Property	Value	Ref.
α_{ICRS}, J2000 [hh mm ss]	08:15:23.30	1
δ_{ICRS}, J2000 [dd mm ss]	-38:59:23.3	1
μ_α [mas yr^{-1}]	-9.692 ± 0.012	1
μ_δ [mas yr^{-1}]	7.349 ± 0.012	1
ϖ [mas]	1.763 ± 0.011	1
Distance [pc]	$567.2^{+6.7}_{-5.9}$	2
G [mag]	13.371 ± 0.003	1
$G_{BP} - G_{RP}$ [mag]	$0.815 \pm XXXX$	1
G_{BP} [mag]	13.697 ± 0.001	1
G_{RP} [mag]	$12.882 \pm XXXXX$	1
J [mag]	12.897 ± 0.026	3
H [mag]	12.431 ± 0.024	3
K [mag]	12.321 ± 0.024	3
u (AB) [mag]	17.63 ± 0.02	4
g (AB) [mag]	16.096 ± 0.008	4
r (AB) [mag]	16.69 ± 0.02	4
i (AB) [mag]	14.123 ± 0.005	4
z (AB) [mag]	14.832 ± 0.011	4
R_* [$R_\odot$]	1.009 ± 0.030	5
[Fe/H] [dex]	0.0 ± 0.23	5
$\log g$ [$\log_{10}$ cm s^{-2}]	4.5 ± 0.25	5
$T_{\rm eff}$ [K]	5900 ± 74	5
m_{bol} [mag]	13.39 ± 0.02	5
$\log(L/L_{bol})$ [dex]	0.046 ± 0.013	5

Notes. References: (1) Gaia EDR3 (Gaia Collaboration et al. 2021), (2) Bailer-Jones et al. (2021), (3) 2MASS (Cutri et al. 2003), (4) SDSS DR8, (5) this work (EEM fits)

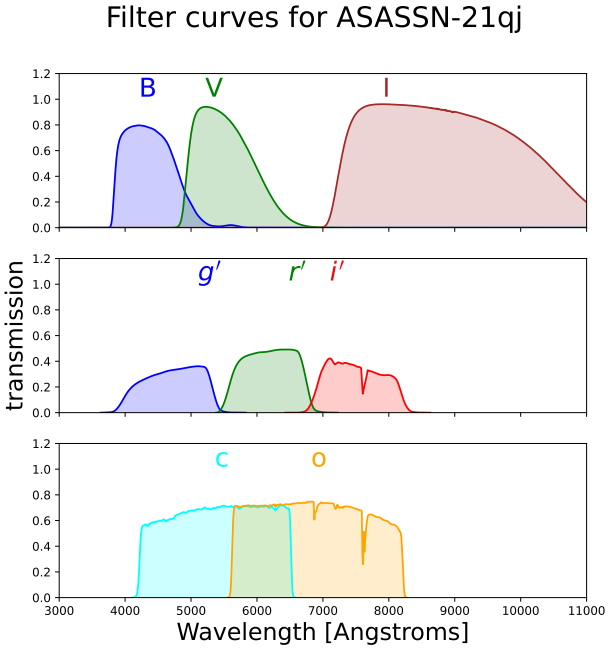

Fig. 1. Filter curves for all telescopes and filters used to observe ASASSN-21qj.

translates to a difference in tangential velocity of $\Delta V_{tan} = 25.37 \pm 0.21$ km s^{-1}. The velocity difference is considerable given the projected separation of 2079 au. Using Kepler's 3rd law, and assuming the observed separation corresponds to the semi-major axis, and the observed ΔV_{tan} corresponded to the full orbital velocity, these quantities would predict a minimum system mass of $> 150\ M_\odot$. Based on the implausible estimated dynamical mass inferred from the observed separation and difference in tangential velocities, we conclude that the visual companion 2MASS J08152298-3859244 is an interloper unrelated to ASASSN-21qj.

3. Observations

The beginning of the eclipse was announced in Rizzo Smith et al. (2021) through the ASASSN survey, which triggered several observing campaigns at optical wavelengths, and an ALMA observation at Band 7 (program `2019.A.00040.S`). The filter passbands for all the observations are shown in Figure 1. A spectrum of the star was obtained with the 2SPOT consortium midway through the eclipse.

3.1. ASAS

The All Sky Automated Survey (ASAS; Pojmanski 1997, 2005; Simon et al. 2018) is a survey consisting of two observing stations - one in Las Campanas, Chile and the other on Maui, Hawaii. Each observatory is equipped with two CCD cameras using V and I filters and commercial f = 200 mm, D = 100 mm lenses, although both larger (D = 250 mm) and smaller (50-72 mm) lenses were used at earlier times. The majority of the data are taken with a pixel scale of $\approx 15''$. ASAS splits the sky into 709 partially overlapping ($9^\circ \times 9^\circ$ fields, taking on average 150 3-minute exposures per night, leading to a variable cadence of 0.3-2 frames per night. Depending on the equipment used and the mode of operation, the ASAS limiting magnitude varied between 13.5 and 15.5 mag in V, and the saturation limit was 5.5 to 7.5 mag. Precision is around 0.01-0.02 mag for bright stars and below 0.3 mag for the fainter ones. ASAS photometry is calibrated against the Tycho catalog, and its accuracy is limited to 0.05 mag for bright, non-blended stars.

3.2. ASAS-SN

The All Sky Automated Survey for Supernovae (ASAS-SN; Shappee et al. 2014; Kochanek et al. 2017) consists of six stations around the globe, with each station hosting four telescopes with a shared mount. The telescopes consist of a 14-cm aperture telephoto lens with a field of view of approximately $4.5^\circ \times 4.5^\circ$ and an $8.0''$ pixel scale. Two of the original stations (one in Hawaii and one in Chile) are fitted with V band filters, whereas the other stations (Chile, Texas, South Africa and China) are fitted with g band filters. ASAS-SN observes the whole sky every night with a limiting magnitude of about 17 mag in the V and g bands.

3.3. ROAD Photometry

The Remote Observatory Atacama Desert (ROAD; Hambsch 2012) is a fully automated telescope located in Chile that obtains nightly photometry in Astrodon B, V and I bands for a wide range of astronomical projects. It consists of a 40-cm $f/6.8$ Optimized Dall-Kirkham and uses a Finger Lakes Instruments camera with a 4k×4k array with pixels of $5\mu m$ in size. Data are reduced using a custom pipeline and then published on the AAVSO website.

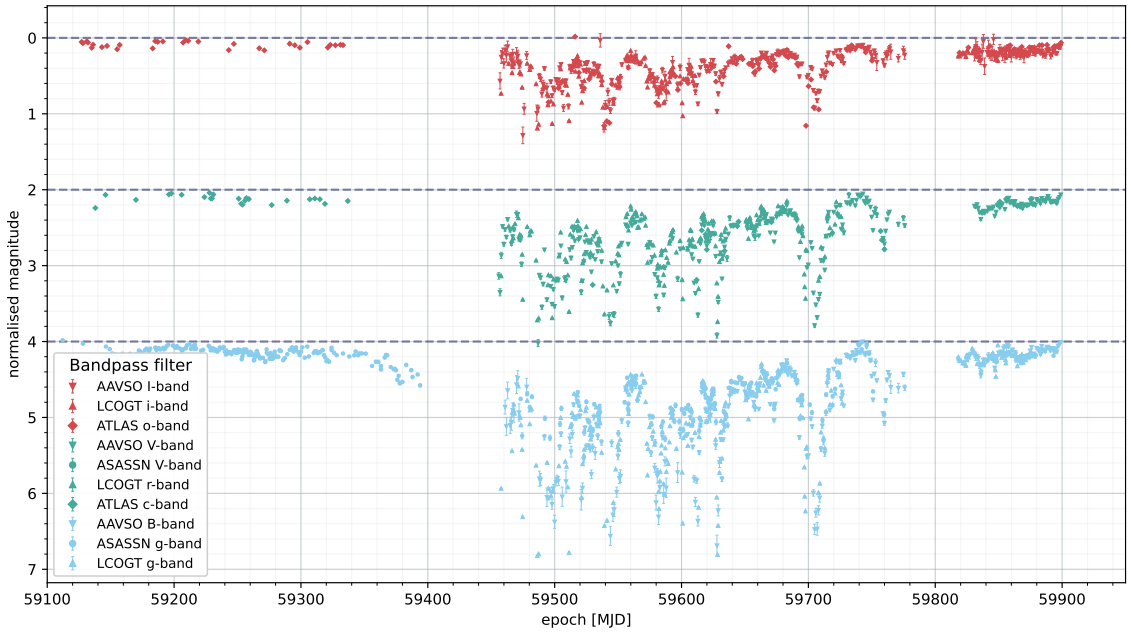

Fig. 2. The light curve of ASASSN-21qj from several different photometric surveys. Three different light curves have been generated by combining data sets with similar passbands for each light curve. The light curves are offset vertically for clarity. The absorption increases from red wavelengths to blue wavelengths.

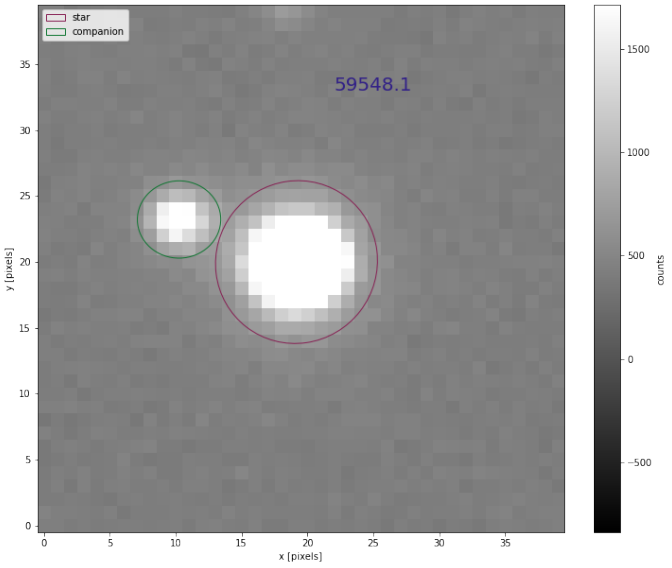

Fig. 3. LCOGT image of ASASSN-21qj taken in the *XXXXg′* band filter. The star is indicated with a red circle, with the visual companion indicated with a green circle.

3.4. NEOWISE photometry

The NEOWISE photometry is presented with the ASASSN *g* light curve in Figure 4.

The Near-Earth Object Wide-field Infrared Survey Explorer (NEOWISE) is a space-based infrared telescope that has been surveying the sky since 2013 at 3.4 and 4.6 μm. NEOWISE orbits near the Earth's day-night terminator, scanning rings of the sky near $\sim$ 90° Solar elongation, and obtains a sequence of observations of a given region of sky every six months. The two wavelength channels are obtained simultaneously through a beamsplitter, allowing for color information to be extracted for each source detected in both bands. For a detailed description of NEOWISE operations and early results from the Reactivation mission see Mainzer et al. (2014), while Cutri et al. (2015) provide a description of the standard data processing and data characteristics. The increase in NEOWISE flux occurred between MJD 58072.27 (UT 2017-11-15) and MJD 58227.48 (UT 2018-04-19).

3.5. LCOGT photometry

Las Cumbres Observatory Global Telescope (LCOGT) is a network of 25 fully robotic operated telescopes distributed over 7 sites located all around the globe. These telescopes are designed to observe transient astronomical events at optical and near-infrared wavelengths. LCOGT provides a large variety of filter options, but the data we collected is in SDSS g, r and i bands. All data is automatically processed and calibrated by the BANZAI pipeline. This process involves bad-pixel masking, bias subtration, dark subtraction, flat field correction, source extraction, astrometric calibration and photometric calibration.

As mentioned in section 2.1, ASASSN-21qj has a visual companion. This caused complications in BANZAIs automatic aperture extraction routine; sometimes correct apertures were extracted for both ASASSN-21qj and the nearby star, and sometimes both sources were extracted in one large aperture, often

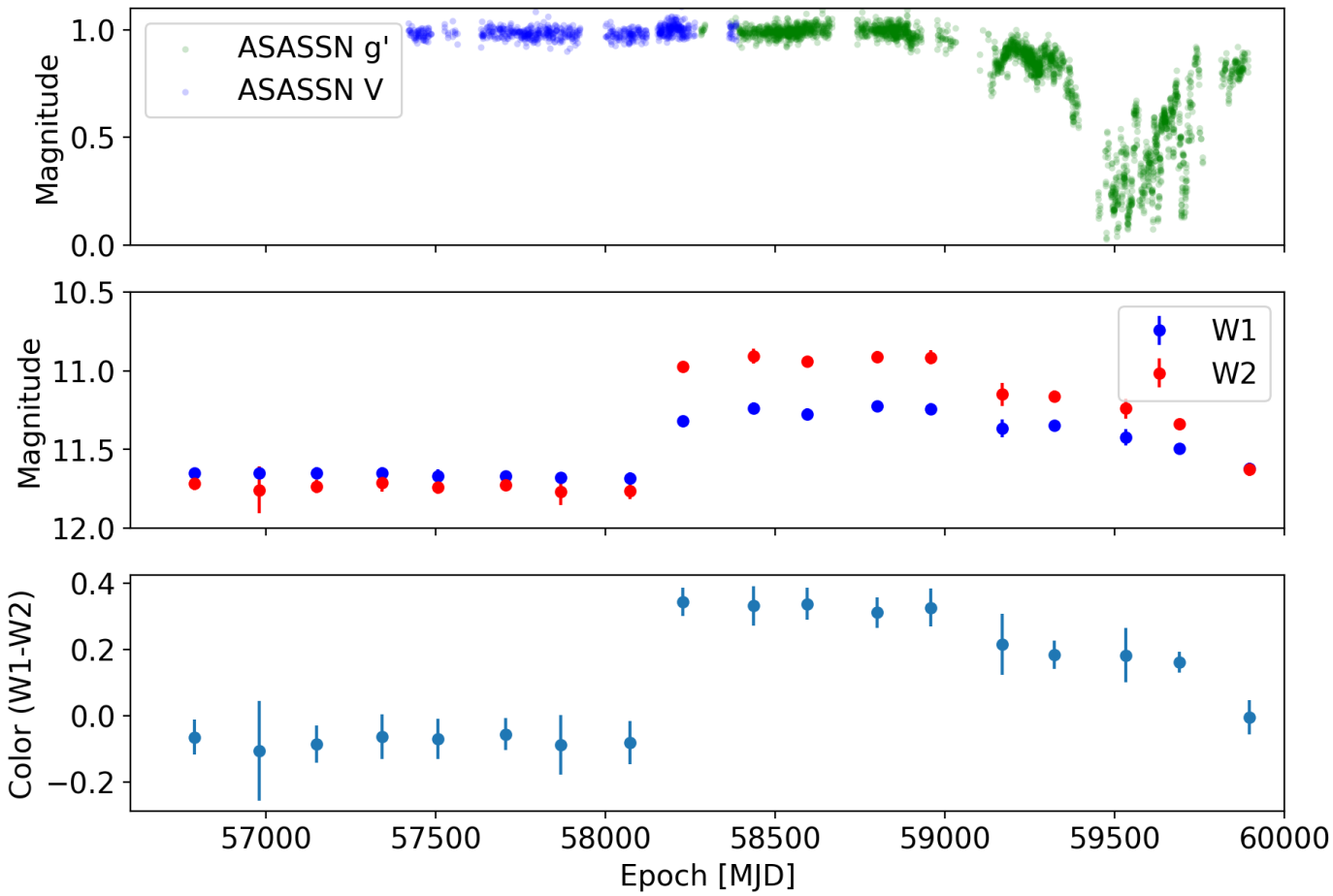

Fig. 4. NEOWISE $W1$ and $W2$ photometry of the star, with the WISE color in the lowest panel. The *NEOWISE* color changes from colourless to very red, which now fades back towards colourless over ~ 500 days.

with an offset from the true center of ASASSN-21qj. Although the companion is faint, this caused the resulting photometry to be in inaccurate and therefor unusable. To correct this, the last two stages of the BANZAI routine, aperture extraction and photometry calibration, were modified for this specific situation.

TODO: see commented notes

3.6. ATLAS

ATLAS is a project that searches for near earth asteroids down to a magnitude of 19 (Tonry et al. 2018). Two filters were obtained, the 'o' (orange) and 'c' (cyan) filters respectively. The data consists of two to four photometric points observed each night when conditions permitted. Photometry with large errors was rejected in a first pass, then the remaining observations during a night were averaged and an error based on the r.m.s. of these nightly points was calculated. The photometry covers the time period where the collision event occurred.

3.7. 2SPOT spectroscopy

A spectrum of the star was taken on 59829.8785 MJD, equal to 2022-09-07 at 08:34:52 UTC, from the Deep Sky Chile[1] site in Chile (at longitude:70°51′11.″86 latitude:30°S 31′34.″71 altitude:1700m AMSL). The telescope is a Ritchey-Chretien telescope (d = 305mm) at $f/5$ (with focal reducer CCD 67 astrophysics) on an equatorial mount GM 3000 HPS from 10 micron[2]. The spectrograph is a Spectrograph Alpy 600 R = 570 with a 23μm wide slit[3] and an ATIK 414ex camera[4]. The spectrum is composed of three unbinned exposures of 1200s each, taken in automatic mode with Prism V11 Software[5], and the spectrum is processed with ISIS software[6]. The final spectrum is shown in Figure 6.

The spectrum shows the absorption features of a typical early G-type star, and apart from the slope which is shaped by the dust absorption, we see no signs of gas absorption in this spectrum, implying that there is only dust in the intervening material.

3.8. ALMA

ADD OBS DATE

The ALMA data from programme `2019.A.00040.S` were downloaded and processed through to a measurement set with CASA (McMullin et al. 2007). These observations used band 7, with a mean wavelength of 880 μm. No source is visible in the default archive products, and we also detect no source at the expected location in CLEAN images. The archive products report an RMS of 17 μJy, and we measure an RMS of 20 mJy in

[1] https://www.deepskychile.com/en/

[2] https://www.10micron.com/en/product/gm3000-hps/

[3] https://www.shelyak.com/produit/alpy-600/?lang=en

[4] https://www.atik-cameras.com/product/atik-414ex/

[5] https://www.prism-astro.com/

[6] http://www.astrosurf.com/buil/isis-software.html

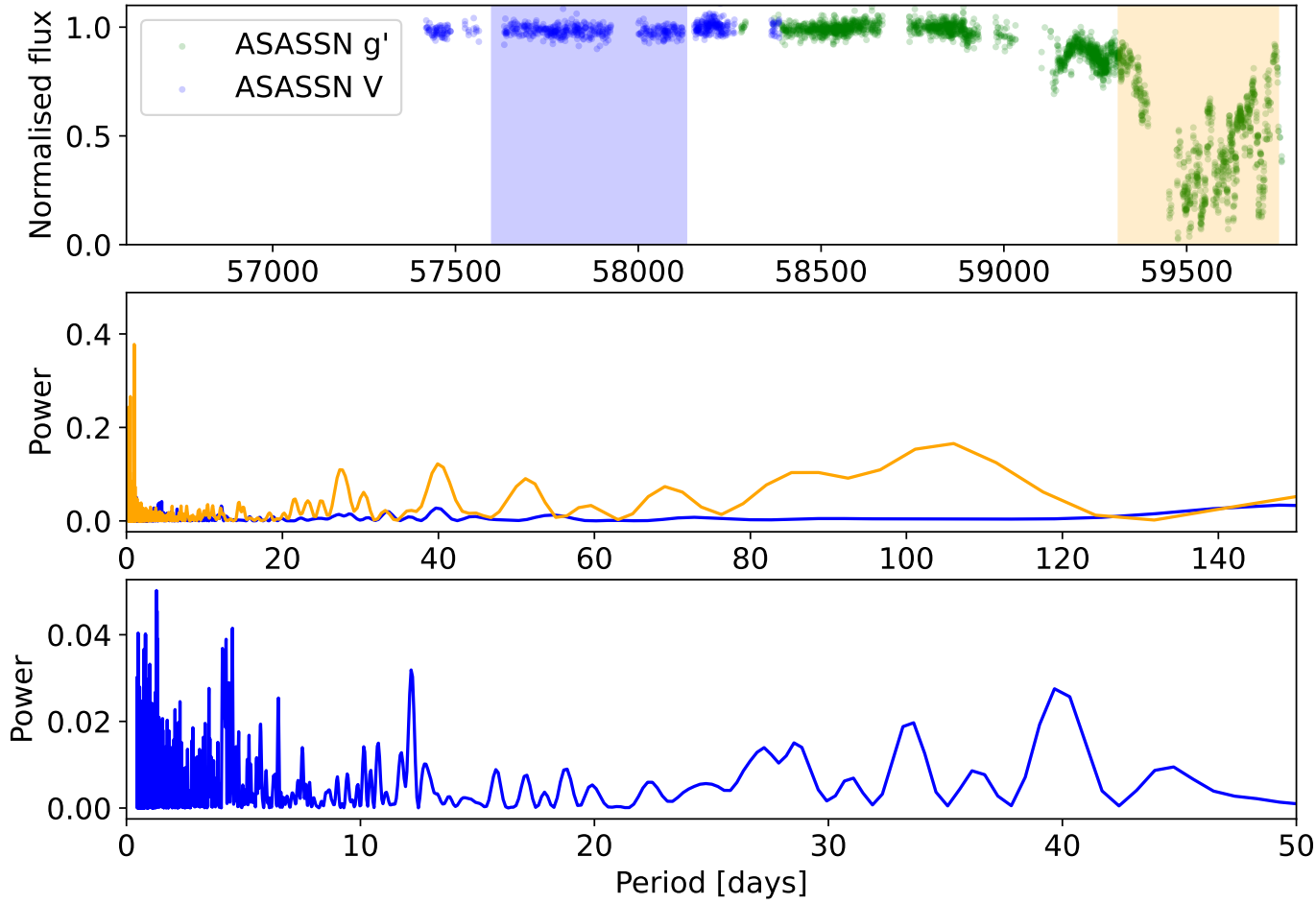

Fig. 5. ASASSN photometry of ASASSN-21qj and the Lomb Scargle periodograms of the photometry in and out of the eclipse. The blue and orange shaded regions in the top panel indicate the range of epochs put into the Lomb Scargle periodogram. Middle panel: The periodograms over a range of 0 to 150 days. Lower panel: The periodogram of the star outside of the eclipse over a range of 0 to 50 days.

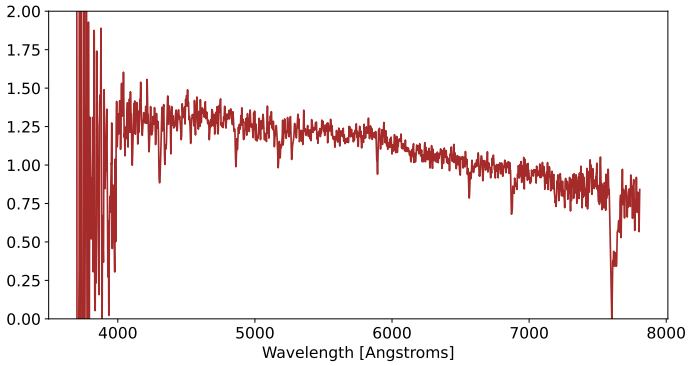

Fig. 6. Spectrum of ASASSN-21qj showing features of a typical G type star.

a naturally weighted image. We therefore consider these results as an upper limit of 60 mJy. In terms of the infrared excess visible in the mid-IR with WISE this upper limit is not at all constraining, but does set limits on emission from cooler dust. These limits are however not particularly constraining for cool dust either, with $L_{\rm dust}/L_\star \gtrsim 10^{-3}$ at ~100 K detectable. For context this level is approximately the level seen for the very bright debris disk around the young A-type star β Pictoris.

4. Analysis

4.1. Dust properties from the colors in the optical

Richelle plots: The photometry shows deeper absorption at bluer wavelengths compared to longer wavelength passbands. This is an indication that the stellar flux is being scattered by particles that are equal to or smaller than the wavelength of light. By plotting the magnitude of the star versus colour (e.g V versus V-I) the particle size and surface density can be determined. Plots of the light curve show reddening consistent with interstellar dust, and this reddening is parameterised with a reddening angle (**Richelle: I'm not sure of the correct name for this!**). The reddening angle for photometry during the eclipse is shown in Figure 7. The measured angle of 59 degrees is consistent with sub-micron sized dust similar in composition to interstellar medium material REF REF RICHELLE.

The sampling of the photometry enables determination of the reddening as a function of time during the eclipse. The reddening is calculated in 20 day bins and plotted in Figure 8, showing that the reddening angle is very consistent over the duration of the eclipse, but that there is a suggestion that the reddening angle changes gradually during the ingress and egress.

TODO: to estimate the minimum mass of all the sub-micron dust in the eclipse and equate that to YYYYY kg of solid material.

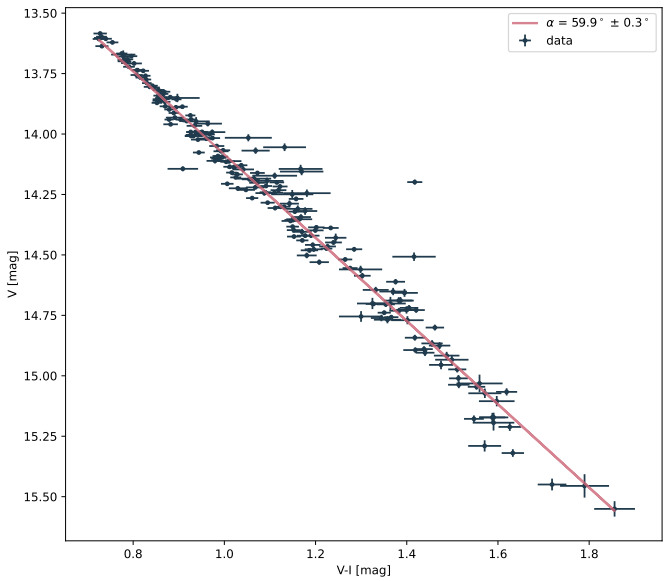

Fig. 7. Plot of V versus V-I colour as measured from AAVSO data. The reddening angle is determined with a straight line fit to the data.

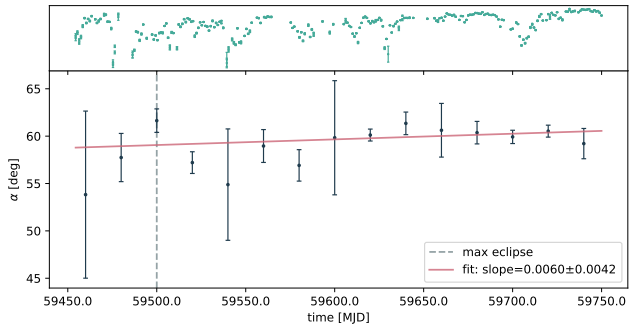

Fig. 8. Plot of reddening angle versus time over the central part of the eclipse. The reddening angle is calculated in 20 day bins. A linear fit is shown over the duration of the eclipse.

4.2. Transverse velocity of the dust cloud

The photometry changes with time, and this is attributed to a cloud of dust moving in front of the stellar disk at a velocity v_{dust} and that has a surface density that changes as a function of position in the dust cloud. A lower bound can be derived for v_{dust} by measuring the gradient of the light curve and determine what velocity a sharp edged and completely opaque occulter moving across the disk of the star would be need to make the same gradient.

We measure the gradient of the light curve in an automated way by fitting straight lines to photometry between nights **(XXX Richelle correct me on this!)** We determine a robust lower limit to the transverse velocity of 5 km s^{-1} for the material moving in front of the star, assuming a radius for the star of 1.009$R_{\odot}$. This means that if the dust is on a circular orbit, it has to be within XXX au (equivalent to an orbital period of YYY years) around the star.

4.3. Frequency analysis of the light curve

We look for any periodicities that could be associated with orbital motion around the star, so we look at the periodogram from 0 to 150 days during the eclipse. As a comparison, we overplot the periodogram for the pre-eclipse light curve as the blue curve in the middle panel. There is some power seen at 40 days which is present in the pre-eclipse light curve, with some (non-significant) periodicities at longer periods.

Looking for periodic stellar activity, the periodogram for the pre-eclipse light curve is shown from 0 to 50 days in the lower panel. Here we see significant periods at around 6.5 and 11 days, which we attribute to light curve modulation caused by starspots rotating in and out of view.

5. Discussion

We have two separate phenomena that occur within 1000 days of each other. Firstly, NEOWISE W1 and W2 photometry shows an approximate doubling of flux in both wavebands, with the longer wavelength showing a larger increase. Observations from the optical bands between the two epochs where the increase occurred have a much higher temporal cadence, but they do not show any corresponding increase in flux. This infrared only increase is consistent with a dust generating event, such as the collision of a planetoid with another planetoid or a terrestrial planet (REF REF). This interpretation is also supported by the reddening of the star during the optical dimming, if we assume that both the optical and IR flux variations are caused by the same dust cloud, then we (discussed further below). The resultant dust cloud has a considerably larger surface area than the progenitors (which were not visible before the IR flux increase), and this dust cloud is then heated by some luminosity source. Typically the host star heats circumstellar dust, but we consider alternative possibilities below.

5.1. Scenario independent constraints

We first consider some scenario independent constraints, as these illustrate some basic problems which are summarised in Figure 9. Most simply, the IR photometry requires very warm dust, but the delay between the IR flux increase and the optical dimming suggests material that is far from the star. While there are other means than stellar luminosity to heat dust, the star is the most conventional source, and requires the dust to be at about 0.1 au given the near-constant temperature of ~1000 K (Fig XXX). A blackbody at this temperature that fits the WISE fluxes implies a dust luminosity of 0.034 $L_{\star}$; that is, assuming blackbody-like absorption and emission 0.034 of the stellar emission is absorbed and re-emitted by the dust. For a dust temperature of 1000 K, the emitting area is 0.01 au^2, equivalent to an object about 7 $R_{\odot}$ in radius. A several-year delay between the IR flux increase and the optical transit, however, implies that the material is on an orbit with a period of at least several years, and hence several au. The duration of the optical transit also suggests a distance of order an au or greater, since closer material would have a period that is shorter than the duration of the transit. Finally, a large orbital distance is also suggested by the gradients in the optical light curve, though the velocities inferred from the gradients are lower limits and hence the material could be closer.

Thus, if the IR and optical flux variations have the same origin, there are basic incompatibilities for scenarios that assume an azimuthally confined clump of orbiting material that is heated by the star. Possible explanations therefore attempt to avoid these restrictions.

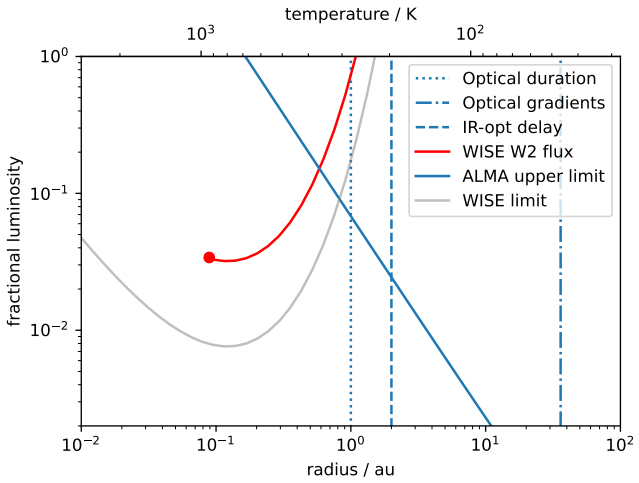

Fig. 9. Model-independent constraints in terms of dust fractional luminosity ($L_{\rm dust}/L_\star$) and stellocentric radius or temperature. The dot shows the location of the dust from an SED fit, and the curved line shows cooler dust that is consistent with the WISE W2 flux alone. The grey line shows what could have been detected with WISE; with detectable emission at a given radius/temperature lying above the grey line. The diagonal line shows the upper limit from the ALMA non-detection. The vertical dotted line shows an approximate lower radial limit on the dust location based on the transit duration. The dashed line a lower radial limit based on the delay between the IR flux increase and optical transit. The vertical solid line shows an upper radial limit based on the optical light curve gradients.

5.2. HYP 1: unrelated phenomena

As discussed below, the observations pose some problems regarding the location of the occulting cloud. The long timescale between the WISE flux increase and the optical dimming, and the gradients in the optical light curve, suggest that the dust is of order au away from the star. This however is contradicted by the hot dust temperature, which would place the dust near 0.1 au. Important here is that the system first came to prominence because of the optical variability, even though subsequent investigation found that the IR flux increase occurred beforehand.

A possible resolution is simply that the WISE flux increase and the optical dimming are unrelated coincidental phenomena. This explanation is unsatisfactory however, because both IR flux increases and dimming events are rare, particularly around stars that are not young. For example, constant near-IR excesses are exceptionally rare among main-sequence stars (1:10,000), and still uncommon for young stars (1:100 Kennedy & Wyatt 2013). In addition, these rates are for 12 *mu*m excesses that are largely constant; rates are lower at shorter wavelengths, and no star has been seen to show an increase from no excess to a sizeable excess (Melis et al. 2012, report a disappearing mid-IR excess, but this is the single example known). Work has shown that young stars that do have unusually bright mid-IR excesses do have a high probability of showing IR flux variability (Meng et al. 2015), which suggests that ASASSN-21qj could be a young system.

Similarly, optical dimming events are also rare for main-sequence stars, for example only one was seen to undergo dust-related optical dimming with Kepler (Boyajian et al. 2016). Young stars that host protoplanetary disks do regularly show optical dimming (known as "dippers"), but these generally have large and constant mid-IR excesses (e.g. Ansdell et al. 2016).

While it is hard to estimate the total probability of observing such a system, we can estimate that the probability of a random star that shows unusual optical dimming also having a mid-IR excess is at best 1% if the system is young, and much lower if it is not. Not all mid-IR excess systems are variable, but quantifying the probability of variability is not simple, so we simply conclude that the coincidental optical and mid-IR flux variation is a best an order 1% event, but probably much less probable.

5.3. HYP 2: dust heated by star

If one insists that the dust is heated by the star, then as noted above it must be relatively close to it; too close for the delay between the IR flux increase and the optical flux decrease to be explained as a fraction of the orbital period. For example, for material at 0.1 au the orbital period is a few weeks. While we may still invoke some singular event to explain the increase in IR flux, e.g. a collision, the new material will rapidly shear azimuthally into a disk, and the optical dimming must then be explained by variation over multiple orbital timescales.

The lack of significant variation in the WISE flux for several years after the increase suggests that this shearing has largely happened within a period of six months. A longer timescale should lead to behaviour that is similar to that seen for stars such as ID8 (Meng et al. 2014), while the material is still shearing and has significant azimuthal variation. Thus, any changes that lead to occultation of the star are more likely related to changes in vertical structure of the disk. Such an increase could be caused by continued dynamical interactions between the massive debris, or excitation by a single larger body (e.g. Ida & Makino 1992).

A possible scenario is therefore that the debris was created in a collisional event involving one or two large bodies, resulting in a sizeable debris cloud. With respect to the collision center of mass, this cloud leaves with at least the escape velocity from the larger body, and is sheared out over tens of orbital periods. The random velocities of the debris cloud objects are then further increased by dynamical interactions ("stirring") both between fragments, and by the original large bodies, the main relevant effect being that the scale height of the disk will slowly increase.

To satisfy the observational constraints, the system must be near to edge-on, such that the disk does not initially block the star. Over time however, the increase in scale height begins to block the star, leading to the slow decrease in optical flux. The depth of the optical dimming implies that the disk was initially radially optically thick. The radial optical depth must now be decreasing and be close to optically thin at both optical and near-IR wavelengths, presumably due to ongoing collisional depletion, to explain the slow return to pre-impact levels. The key difference for this model is that there is not a discrete cloud of debris slowly passing in front of the star, and that the star's return to normal flux is instead related to collisional depletion.

As above, this model has problems. For example, if the material is on an orbit at 0.1 au, structures passing in front of the star should have transverse velocities of about 100 km s^{-1}, significantly faster than inferred from the light curves. This issue is circumvented by asserting that the structures are sufficiently large and "fluffy" that the gradients are more related to the density gradients in the occulting structures than their velocity. There may also be a problem with the strong variation in the optical light curves; a disk that has undergone significant collisional evolution should have reached a quasi-steady state, where objects of all sizes from the largest bodies to smallest dust grains are all colliding on their respective timescales, which should mean that clumpy structure related to individual parent bodies has largely been erased. The geometry of the disk in this scenario may also be fine tuned, in that a radially optically thick disk may also block IR emission from the inner disk, which is incompatible

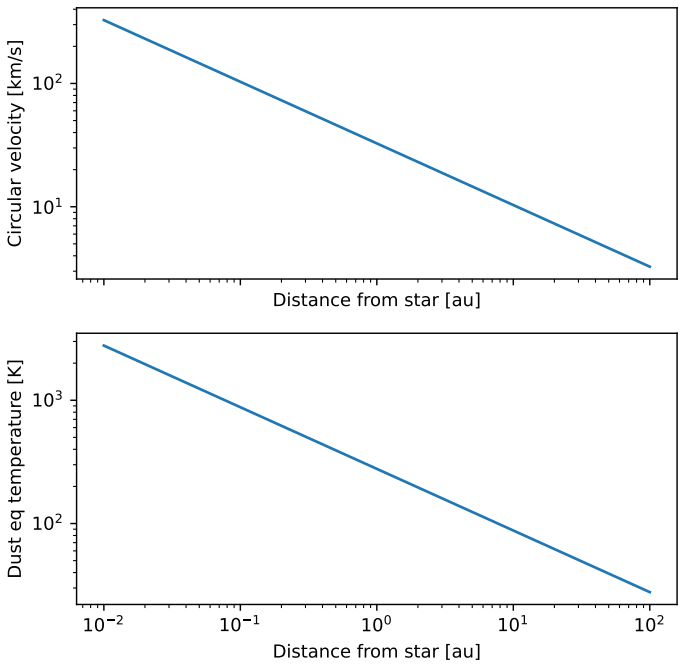

Fig. 10. Circular velocity as a function of semimajor axis, and the effective temperature of dust as a function of semi-major axis.

with the warm emission. This problem can however be avoided if the disk is optically thick enough to block the star at optical wavelengths, but remains reasonably optically thin at near-IR wavelengths.

5.4. HYP 3: dust heated by synestia/collision

If we assume that the dust cloud expanded from a point source out into a star-facing circular optically thin disk with area A_{IR} and radius r_{IR} in a time t_{IR} (where this time has an upper limit of 6 months corresponding to the duration between the NEOWISE epochs), then we can estimate a linear velocity $v_{IR}t_{IR} = r_{IR}$ for the expansion of the cloud of:

$$v_{IR} = \frac{r_{IR}}{t_{IR}} = \frac{0.35 r_{IR}}{t_{IR}} =$$

A figure showing the temperature dependency is is Figure 10.

One advantage of this hypothesis is that we are no longer tied to surface area/distance from star challenge, and that the derived circular velocities from the light curve gradients can be made consistent with an orbit out at Jupiter/Saturn distances. We therefore require a new energy source to heat the dust - we note that the gravitational binding energy of two large terrestrial planets colliding can produce enough energy over one year to explain the observed energy flux, but problems with keeping the rapidly expanding clouds of dust warm enough for the thermal emission remain. One possible intriguing explanation is that we are seeing the formation of a synestia - this is a hypothesised structure thought to exist just after the collision that would subsequently form the Moon REF LANE. A synestia is a silicate rich luminous object with an effective temperature of over a thousand Kelvin and a diameter on the order of 200,000 km. This could provide a heating source for the optically thin dust cloud surrounding it for the duration of the observations. Long wavelength spectroscopy could reveal emission or absorption features of silicates from the synestia, confirming the existence of these objects.

6. Conclusions

Probing disintegrating planetary material has been proven to be a very useful method to access the composition of building blocks of planets outside of the Solar System. E.g. the disintegration of a gas giant around a white dwarf was used to infer its composition (Gänsicke et al. 2019). White dwarf star pollution has also yielded insights about refractory (Fe/Mg/Ca) element content of rocky material around such stars (Turner & Wyatt 2020; Putirka & Xu 2021; Blouin 2020). See also Veras (2021) for a review.

Planets and asteroids falling into white dwarfs, however, haven been probably heavily processed during the late stellar evolution. The unusually warm dust passing in front of a young star presented in this work, on the other hand, may allow to probe the interior of planetesimals in the early stages of planet formation. The eclipse is expected to last for another 200 days, allowing us to perform further spectroscopic analysis of the dust in this system.

1. There was a collision between planetoids towards ASASSN-21qj which generated a debris cloud.
2. The cloud moved in front of the star, and we have a fresh measure of the debris from a collision.
3. Probing dust of material in the early stages of planet formation is complementary to studies of white dwarf polluters. The latter represent planetary material after the end of the main sequence of the host star.

Future observations include IR high contrast imaging in order to see if the 4-5 microns excess is a point source or is now extended. A disk of dust that is about 1au in length has an angular size of 20 millarcsec at the distance of ASASSN-21qj. This can be marginally resolved with K band imaging with an 8m class telescope with a high contrast imager such as ERIS. The same camera can carry out integral field spectroscopy of this system, and search for silicate absorption in the transmitted light spectra, if carried out before the end of the eclipse.

If the collision remnant has not been completely destroyed, orbital motion over the next five to ten years will place it at about 50 milliarcseconds from the star, marginally resolvable with ERIS. This star is a prime target for longer wavelength observations, such as MIRI with the JWST.

The prospect of detecting more of these systems is increasing, with the large scale surveys and triggers provided by ASAS-SN, and when the LSST sees first light, the detection and selection of stars to study will be triggered by all sky observations such as these. Combined with J1407, PDS 110, and several other transiting extended disks, these present an opportunity to study with unprecedented angular resolution the substructure of debris clouds from terrestrial planet collision, and the substructure of circumplanetary disks that are home to exomoon formation, providing an additional detection and characterisation channel. The next decade will result in the detection of several dozen of these transiting systems, and having ephemerides for systems that show repeated eclipses will enable targeted observing campaigns.

Acknowledgements. This research has used the SIMBAD database, operated at CDS, Strasbourg, France (Wenger et al. 2000). This work has used data from the European Space Agency (ESA) mission *Gaia* (https://www.cosmos.esa.int/gaia), processed by the *Gaia* Data Processing and Analysis Consortium (DPAC, https://www.cosmos.esa.int/web/gaia/dpac/consortium). Funding for the DPAC has been provided by national institutions, in particular the institutions participating in the *Gaia* Multilateral Agreement. To achieve the scientific results presented in this article we made use of the *Python* programming language[7], especially the *SciPy* (Virtanen et al. 2020),

[7] Python Software Foundation, https://www.python.org/

NumPy (Oliphant 2006), *Matplotlib* (Hunter 2007), *emcee* (Foreman-Mackey et al. 2013), and *astropy* (Astropy Collaboration et al. 2013, 2018) packages. We acknowledge with thanks the variable star observations from the AAVSO International Database contributed by observers worldwide and used in this research. We thank the Las Cumbres Observatory and its staff for its continuing support of the ASAS-SN project, and the Ohio State University College of Arts and Sciences Technology Services for helping us set up and maintain the ASAS-SN variable stars and photometry databases. ASAS-SN is supported by the Gordon and Betty Moore Foundation through grant GBMF5490 to the Ohio State University and NSF grant AST-1515927. Development of ASAS-SN has been supported by NSF grant AST-0908816, the Mt. Cuba Astronomical Foundation, the Center for Cosmology and AstroParticle Physics at the Ohio State University, the Chinese Academy of Sciences South America Center for Astronomy (CASSACA), the Villum Foundation, and George Skestos. Early work on KELT-North was supported by NASA Grant NNG04GO70G. Work on KELT-North was partially supported by NSF CAREER Grant AST-1056524 to S. Gaudi. Work on KELT-North received support from the Vanderbilt Office of the Provost through the Vanderbilt Initiative in Data-intensive Astrophysics. Part of this research was carried out in part at the Jet Propulsion Laboratory, California Institute of Technology, under a contract with the National Aeronautics and Space Administration (80NM0018D0004). This publication makes use of VOSA, developed under the Spanish Virtual Observatory project supported by the Spanish MINECO through grant AyA2017-84089. This publication makes use of VOSA, developed under the Spanish Virtual Observatory[8] project funded by MCIN/AEI/10.13039/501100011033/ through grant PID2020-112949GB-I00. VOSA has been partially updated by using funding from the European Union's Horizon 2020 Research and Innovation Programme, under Grant Agreement 776403 (EXOPLANETS-A). This work has made use of data from the Asteroid Terrestrial-impact Last Alert System (ATLAS) project. The Asteroid Terrestrial-impact Last Alert System (ATLAS) project is primarily funded to search for near earth asteroids through NASA grants NN12AR55G, 80NSSC18K0284, and 80NSSC18K1575; byproducts of the NEO search include images and catalogs from the survey area. This work was partially funded by Kepler/K2 grant J1944/80NSSC19K0112 and HST GO-15889, and STFC grants ST/T000198/1 and ST/S006109/1. The ATLAS science products have been made possible through the contributions of the University of Hawaii Institute for Astronomy, the Queens University Belfast, the Space Telescope Science Institute, the South African Astronomical Observatory, and The Millennium Institute of Astrophysics (MAS), Chile.

References

Ansdell, M., Gaidos, E., Rappaport, S. A., et al. 2016, ApJ, 816, 69
Astropy Collaboration, Price-Whelan, A. M., Sipőcz, B. M., et al. 2018, AJ, 156, 123
Astropy Collaboration, Robitaille, T. P., Tollerud, E. J., et al. 2013, A&A, 558, A33
Bailer-Jones, C. A. L., Rybizki, J., Fouesneau, M., Demleitner, M., & Andrae, R. 2021, AJ, 161, 147
Bayo, A., Rodrigo, C., Barrado Y Navascués, D., et al. 2008, A&A, 492, 277
Blouin, S. 2020, MNRAS, 496, 1881
Boyajian, T. S., LaCourse, D. M., Rappaport, S. A., et al. 2016, MNRAS, 457, 3988
Cutri, R. M., Mainzer, A., Conrow, T., et al. 2015, Explanatory Supplement to the NEOWISE Data Release Products, Explanatory Supplement to the NEOWISE Data Release Products, <A href="http://wise2.ipac.caltech.edu/docs/release/neowise/expsup"> http://wise2.ipac.caltech.edu/docs/release/neowise/expsup</A>
Cutri, R. M., Skrutskie, M. F., van Dyk, S., et al. 2003, VizieR Online Data Catalog, 2246, 0
Foreman-Mackey, D., Hogg, D. W., Lang, D., & Goodman, J. 2013, PASP, 125, 306
Gaia Collaboration, Brown, A. G. A., Vallenari, A., et al. 2021, A&A, 649, A1
Gänsicke, B. T., Schreiber, M. R., Toloza, O., et al. 2019, Nature, 576, 61
Hambsch, F.-J. 2012, Journal of the American Association of Variable Star Observers (JAAVSO), 40, 1003
Hunter, J. D. 2007, Computing in Science and Engineering, 9, 90
Ida, S. & Makino, J. 1992, Icarus, 96, 107
Jackson, A. P. & Wyatt, M. C. 2012, MNRAS, 425, 657
Jackson, A. P., Wyatt, M. C., Bonsor, A., & Veras, D. 2014, MNRAS, 440, 3757
Kennedy, G. M. & Wyatt, M. C. 2013, MNRAS, 433, 2334
Kochanek, C. S., Shappee, B. J., Stanek, K. Z., et al. 2017, Publications of the Astronomical Society of the Pacific, 129, 104502
Mainzer, A., Bauer, J., Cutri, R. M., et al. 2014, ApJ, 792, 30
McMullin, J. P., Waters, B., Schiebel, D., Young, W., & Golap, K. 2007, in Astronomical Society of the Pacific Conference Series, Vol. 376, Astronomical Data Analysis Software and Systems XVI, ed. R. A. Shaw, F. Hill, & D. J. Bell, 127
Melis, C., Zuckerman, B., Rhee, J. H., et al. 2012, Nature, 487, 74
Meng, H. Y. A., Su, K. Y. L., Rieke, G. H., et al. 2015, ApJ, 805, 77
Meng, H. Y. A., Su, K. Y. L., Rieke, G. H., et al. 2014, Science, 345, 1032
Oliphant, T. E. 2006, A guide to NumPy, Vol. 1 (Trelgol Publishing USA)
Pojmanski, G. 1997, Acta Astronomica, 47, 467
Pojmanski, G. 2005, VizieR Online Data Catalog (other), 0050, J/other/AcA/50
Putirka, K. D. & Xu, S. 2021, Nature Communications, 12, 6168
Rizzo Smith, M., Jayasinghe, T., Stanek, K. Z., et al. 2021, The Astronomer's Telegram, 14879, 1
Rizzo Smith, M., Rowan, D. M., Hambsch, F. J., et al. 2022, The Astronomer's Telegram, 15531, 1
Shappee, B. J., Prieto, J. L., Grupe, D., et al. 2014, The Astrophysical Journal, 788, 48
Simon, J. D., Shappee, B. J., Pojmanski, G., et al. 2018, VizieR Online Data Catalog, J/ApJ/853/77
Su, K. Y. L., Jackson, A. P., Gáspár, A., et al. 2019, AJ, 157, 202
Su, K. Y. L., Kennedy, G. M., Schlawin, E., Jackson, A. P., & Rieke, G. H. 2022, ApJ, 927, 135
Tonry, J. L., Denneau, L., Heinze, A. N., et al. 2018, PASP, 130, 064505
Turner, S. G. D. & Wyatt, M. C. 2020, MNRAS, 491, 4672
Veras, D. 2021, in Oxford Research Encyclopedia of Planetary Science, 1
Virtanen, P., Gommers, R., Oliphant, T. E., et al. 2020, Nature Methods, 17, 261
Wenger, M., Ochsenbein, F., Egret, D., et al. 2000, A&AS, 143, 9

[8] https://svo.cab.inta-csic.es